

Article

Measurement and Modelling of Leakage Current Behaviour in ZnO Surge Arresters under Various Applied Voltage Amplitudes and Pollution Conditions

Nurul A. A. Latiff ¹, Hazlee A. Illias ^{1,*} , Ab H. A. Bakar ² and Sameh Z. A. Dabbak ¹

¹ Department of Electrical Engineering, Faculty of Engineering, University of Malaya, Kuala Lumpur 50603, Malaysia; ainlatiff@gmail.com (N.A.A.L.); al_dabak@hotmail.com (S.Z.A.D.)

² UM Power Energy Dedicated Advanced Centre (UMPEDAC), Level 4, Wisma R&D UM, University of Malaya, Jalan Pantai Baharu, Kuala Lumpur 59990, Malaysia; a.halim@um.edu.my

* Correspondence: h.illias@um.edu.my; Tel.: +60-3-7967-4483

Received: 21 March 2018; Accepted: 5 April 2018; Published: 9 April 2018



Abstract: In zinc oxide (ZnO) surge arresters, leakage current usually flows across the arrester under normal operating condition. Leakage current is one of the factors which contribute towards degradation of surge arresters and therefore, it is very important to monitor the condition of surge arrester. In this work, the behaviour of leakage current in a ZnO surge arrester during normal operation, under different voltage amplitudes, wetness and pollution conditions was analysed. An 11 kV surge arrester model in three-dimensional space was subjected to finite element analysis (FEA) to determine the leakage current under different conditions. The results from the FEA model were compared with the measurement results to validate the model that has been developed. From comparison between the measurement and simulation results, physical parameters of a surge arrester that influence the leakage current under different conditions of the surge arrester were identified from the model. Through this work, a better understanding of leakage current behaviour can be attained, which may help in condition monitoring analysis on surge arrester in electrical utilities.

Keywords: surge arrester; leakage current; finite element analysis; zinc oxide; harmonic analysis

1. Introduction

Transmission tower protection is important in protecting electrical equipment from damage [1,2]. A natural phenomenon that usually happens on transmission towers is lightning overvoltage [3,4]. One of the ways to protect the transmission line from lightning overvoltage is by installing surge arresters [5,6]. A surge arrester limits the peak overvoltage to a level which will protect the instrument from damage [7]. The degradation of ZnO surge arresters is caused by many factors, but one of the main ones is moisture ingress due to weakening of the housing sealing which can lead to internal discharges [8], increasing of electric field around the surge arrester [9] and overheating of the surge arrester.

Since 1965 many types of surge arresters are available [10]. The usual types of surge arresters are silicon carbide arresters with spark gaps, silicon carbide arresters with current limiting gaps and gapless metal oxide arresters. Unfortunately, arresters with spark gaps are not very suitable to limit the switching overvoltage. Therefore, new developments in solid state technology have led to the development of non-linear resistors. With this new technology, new class of surge arresters named zinc oxide (ZnO) surge arresters has been developed, which offer a lot of improvements and advantages over other arrester types [11,12].

A leakage current always flows across arresters under normal condition. Leakage currents can be categorised as resistive and capacitive component currents. Capacitive component currents are due to the grading capacitor, stray capacitance or permittivity of the ZnO elements. Resistive components are due to pollution of ZnO elements. The resistive current will increase with time, ambient temperature and applied voltage [13,14]. Thus, it is very important to monitor the leakage current behaviour in order to reduce the degradation of ZnO surge arresters. Since leakage currents are influenced by various surge arrester parameters, many studies have been performed on the leakage current behaviour under many circumstances. In general, these can be divided into two methods: off-line and on-line.

Among these methods, a helpful indication of the surge arrester condition is based on the calculation of its resistive current [15–17]. Measurements of capacitive and resistive leakage currents have become important since the past. Therefore, several methods for extracting resistive leakage current from the total leakage current have been proposed by many academics. There are the point-on-wave method (POWM) [18], current compensation method (CCCM) [17,19,20], current orthogonality method (COM) [16], resistive current waveshape-based method (RCWM) [21], harmonic analysis method (HAM), time delay addition method (TDAM) and improved time delay addition method (ITDAM) [22].

In this work ITDAM was used. ITDAM was chosen since it is more accurate compared to other previous algorithms. This method is capable of extracting resistive and capacitive currents under applied harmonic voltages and based on the study, ITDAM can be utilized in offline or online measuring processes. This technique is based on the orthogonality between resistive and capacitive currents. The advantage of this method is that the harmonic components of the applied voltage are not ignored, where the resistive current is extracted from the total leakage current under applied harmonic voltages. This method has also been used to study the main factors of leakage current variation and the influence of leakage current on UV aging and pollution [23,24].

Although many studies on surge arrester leakage current have been performed in the past, modelling of surge arresters using actual physical dimensions is less likely to be found in literature. Thus, a three-dimensional (3D) 11 kV surge arrester model was developed in a finite element method (FEM) and was employed to simulate the leakage current in different conditions of the applied voltage, wetness and pollution. Measurements of surge arrester leakage current under different conditions were also conducted. They were used to compare with the simulation results to validate the FEA model. Through comparison between measurement and simulation results, a greater understanding on surge arrester leakage current behaviour can be attained and physical parameters of a surge arrester that influence the leakage current under various surge arrester conditions can be identified from the model.

2. Proposed Methodology

This section describes in details the development of the models in finite element analysis (FEA), leakage current measurement setup, preparation of the test samples, leakage current calculation using FEA model and extraction method of resistive leakage current. The dimensions and parameters of the ZnO surge arrester used in this work are shown in Table 1.

Table 1. Dimensions and parameters of the surge arrester.

Characteristics	Data
Creepage distance	344 mm
Dimensions (L × B × H)	39 × 29 × 26 cm
Height	227 mm
Housing material	Silicon rubber
MCOV	10 kV _{rms}
Net weight	1.86 kg
Nominal discharge current, I _n 8/20 μs	10 kA peak
Number of sheds	4
Rated voltage	12.5 kV _{rms}

2.1. Leakage Current Measurement Setup

Figure 1 shows the leakage current measurement setup on the ZnO surge arrester used in the laboratory. The measurement setup consists of a sinusoidal variable voltage source, a high voltage step-up transformer (T_x) of 0.22/100 kV, a 2.4 M Ω protective resistor (R_s) to prevent short circuit, a 1 nF measuring capacitor (C_1) to observe the applied voltage, a measuring circuit, a 20 k Ω shunt resistor (R_{sh}) to measure the leakage currents by measuring the voltage drop from the current built across the resistance and a two channel digital storage oscilloscope to capture the applied voltage and current through a silicone rubber-housed surge arrester.

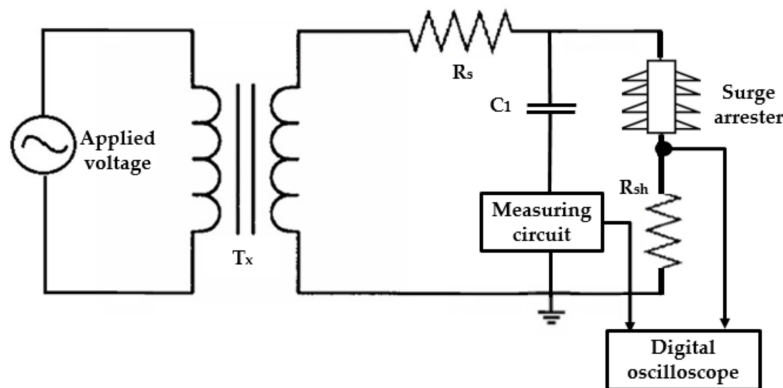


Figure 1. Experimental setup for leakage current measurement.

Measurements of surge arrester leakage current were conducted under different applied voltages and conditions, as summarised in Table 2. For test sample 1, the applied voltage amplitude of 50 Hz AC sinusoidal was varied at 6, 6.5, 7, 7.5, 8, 8.5, 9, 9.5 and 10 kV while maintaining its temperature at 26 °C. The surge arrester was stressed for 30 min at 5 kV_{rms} before any measurement was taken to ensure that quasi-static conditions were reached. One of the objectives of this work was to inspect the effect of pollution on the leakage current of the surge arrester. Hence, test samples 2 and 3 were prepared based on the pollution related to natural and anthropogenic sources. For test sample 2, the uncontaminated arrester was sprayed with water on the arrester surface. Different wetnesses of the arrester were generated by adding water on the arrester surface in different quantity and the testing was under an applied voltage of 8 kV_{rms} at 26 °C.

For test sample 3, the surge arrester was polluted by anthropogenic sources. The outer layer of the surge arrester was contaminated with dry sand, wet sand, salt sand and salt water and tested under an applied voltage of 50 Hz, 8 kV_{rms} at 26 °C. The wet sand was prepared by adding 200 g of sand into 150 mL of distilled water. The salt sand was a combination of 50 g of NaCl and 100 g of sand while for salt water, the solution consists of 50 g NaCl and 50 mL distilled water. For every pollution type, the arrester was cleaned and rinsed with water thoroughly before another type of pollution was applied. At the end of the experiment, the leakage current waveform recorded by the oscilloscope was used to extract the resistive and capacitive current using an improved time-delay addition method (ITDAM), which has been explained in Section 2.3 [22].

Table 2. Conditions of each test sample.

Test Sample	Condition		
	Applied Voltage Amplitude	Temperature	Surface Condition
1	50 Hz AC sinusoidal: 6, 6.5, 7, 7.5, 8, 8.5, 9, 9.5 and 10 kV _{rms}	26 °C	Clean
2	50 Hz, 8 kV _{rms} AC sinusoidal	26 °C	Dry, lightly wet, wet, very wet
3	50 Hz, 8 kV _{rms} AC sinusoidal	26 °C	Clean, dry sand, wet sand, salt sand and salt water

2.2. Finite Element Analysis (FEA) Leakage Current Model

A three-dimensional, 11 kV ZnO surge arrester model was developed in finite element analysis as depicted in Figure 2. The FEA software used was COMSOL Multiphysics (COMSOL Inc., Stockholm, Sweden). The model was developed according to the exact dimensions of the surge arrester that was used in the measurement. The arrester comprises two ZnO blocks, a glass layer between the insulation and ZnO and aluminium caps at each end. The insulation material is made of silicone rubber and the whole model geometry was surrounded by a layer of air.

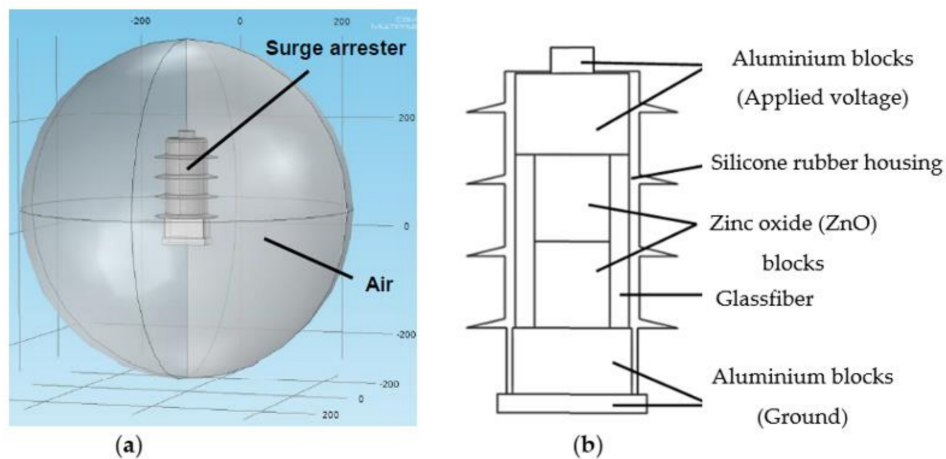


Figure 2. Surge arrester model; (a) drawn in 3D; (b) detailed structure of the model.

The electrical conductivity, σ and relative permittivity, ϵ_r of each material in the model were assigned as listed in Table 3. Since ZnO is a nonlinear element, the electrical conductivity of the ZnO blocks was assigned according to the measured V-I characteristics curve of the surge arrester during normal conditions, as shown in Figure 3, where their electrical conductivity is voltage-dependent. This curve is a fundamental approach in displaying the changes of resistance as a function of the voltage [25]. Generally, the ZnO varistors spend their whole life in this region where conduction is very near to zero by means there is minimal leakage current flowing through the arrester.

Table 3. Properties of each material in the model.

Material	Relative Permittivity, ϵ_r	Electrical Conductivity, σ (S/m)
Air	1	0
Silicone rubber	11.7	1×10^{-12}
Zinc Oxide	2250	From V-I curve
Glass	4.2	1×10^{-14}
Aluminium	1	3.77×10^7

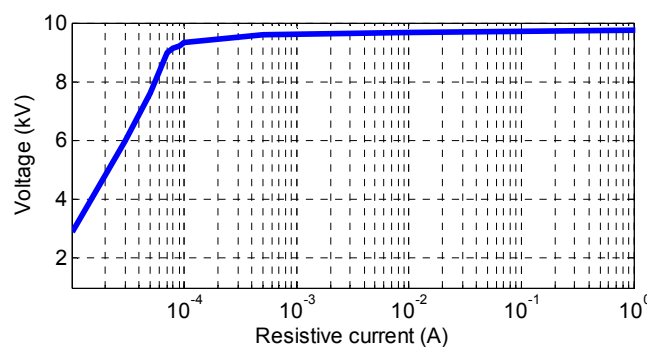


Figure 3. V-I characteristics curve of ZnO varistor.

The boundary conditions of the model were set with relevant interface settings as shown in Table 4. A voltage with the presence of harmonic components was applied to the terminal of the arrester while the bottom of the arrester was grounded, whereby zero electric potential was applied. The outer side of the arrester was enclosed by air. All interior boundaries were set to continuity.

After the boundary and material of the model were assigned, the model was meshed. The FEA model estimates the solution of domain, boundary, edge and point of surge arrester model by using some elementary shape functions, which include tetrahedral, triangular, edge and vertex elements. The shape function can be either constant, linear, or of higher order. In order to obtain accurate results, a finer or coarser mesh is required depending on the element order in the surge arrester model. Since the size of the triangular elements has substantial effect on the simulation time, the size of the triangular elements used was normal for air, finer for all domains of the model except for ZnO, which is extremely fine because it is the important element of the model. While constraining the potential on edges, it can produce a current outflow that is mesh-dependent [26–29]. The meshing elements of the surge arrester are shown in Figure 4.

Table 4. Boundary settings of the model.

Boundary	Boundary Condition	Expression
Terminal	Applied voltage	$V = V_0 + \sum_{k=1}^K V_k \sin(k\omega t + \alpha_k)$
Air	Electric insulation	$n \cdot J = 0$
Ground	Zero electric potential	$V = 0$
All interior boundary	Continuity	$n \cdot (J_1 - J_2) = 0$

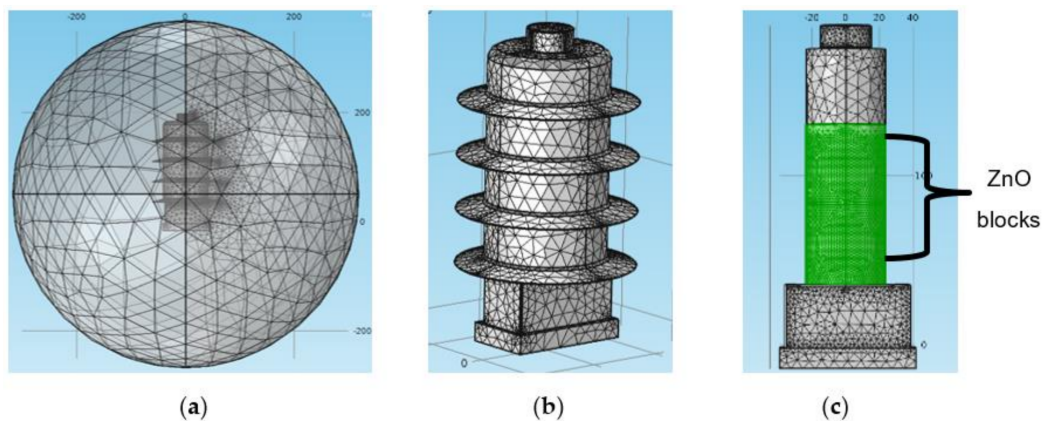


Figure 4. Meshing elements in the model; (a) normal elements for air; (b) finer elements for all domains of surge arrester; (c) extremely fine elements for ZnO.

The geometry of the surge arrester model was solved using partial differential equations (PDEs). The module employed in the model is the electric current module to obtain the electric field and current density distributions on the surge arrester. The leakage current was calculated through surface integration of the current density, which was attained on the ground surface. Equations (1)–(5) were used by the FEA model to solve the problem as follows:

$$\nabla \cdot J = Q_j \quad (1)$$

$$J = \left(\sigma + \varepsilon_0 \varepsilon_r \frac{\partial}{\partial t} \right) E + J_e \quad (2)$$

where J is the current density, Q_j is the current source, ε_r is the relative permittivity of the material, σ is the electrical conductivity, E is the electric field, J_e is the externally generated current density, which equals to zero in the surge arrester model and V is the electric potential.

The problem to be solved in the model is governed by Maxwell's equation as follows:

$$\nabla \times E + \frac{\partial B}{\partial t} = 0 \quad (3)$$

By applying quasi-static assumptions, Equation (3) becomes:

$$\nabla \times E = 0 \quad (4)$$

Since the electric field E is conservative and irrotational, E can be written as:

$$E = -\nabla V \quad (5)$$

2.3. Leakage Current Extraction Method

There are several techniques to compute the value of resistive leakage current from the total leakage current. The method used to extract resistive leakage current in this study is the improved time delay addition method (ITDAM) [22]. This technique is based on the orthogonality between resistive and capacitive currents. The advantage of this method is that the harmonic components of the applied voltage are not ignored. The resistive and capacitive currents are extracted from the total leakage current under applied harmonic voltages. The capacitive current is attained by shifting the total leakage current by 90° . Then, the resistive leakage current is obtained by subtracting the capacitive leakage current from the total leakage current. In this method, only the third and fifth harmonics of the applied voltage were measured. Since the upper harmonics comprise of only small values, they are not considered. The steps used for this method is shown in Figure 5 and describe as follows:

Step 1: Obtaining signals

The first step in extracting the resistive leakage current using ITDAM is obtaining the signals of applied voltage and total leakage current of the measurement and simulation.

Step 2: Determine the phase angles and amplitudes of current signals

The Fast Fourier Transform (FFT) was used to determine the phase angles and amplitudes of total leakage current to the measured current signal ($I_{t1m} - \theta_{1i}, I_{t3m} - \theta_{3i}, I_{t5m} - \theta_{5i}$).

Step 3: Determine the phase angles of voltage signals

The phase angle of voltage harmonics was determined by applying FFT to the voltage signals ($\theta_{1v}, \theta_{3v}, \theta_{5v}$).

Step 4: Shifting the phase leakage current

The lagging phase ($2\theta_{1i} - 2\theta_{1v}$) was used to shift I_{t1} .

Step 5: Inserting the phase shifted leakage current

I_{t1} was inserted with the phase-shifted leakage current ($I_{t1shifted}$).

Step 6: Determine the peak time

The peak time of added current waveforms (T_{p1}) was determined.

Step 7: Obtaining the capacitive leakage current

Based on the T_{p1} , the fundamental harmonic peak value of the capacitive leakage current (I_{c1m}) can be obtained from the I_{t1} waveform. The fundamental capacitive leakage current is formed as follows:

$$I_{c1}(t) = I_{c1m} \cos(\omega t + \theta_{1v}) \quad (6)$$

Step 8: Repeat steps 4 to 7

For other harmonics, steps 4 to 7 were repeated.

Step 9: Attaining the resistive leakage current

The fundamental, third and fifth capacitive currents were added and capacitive current was obtained. Finally, by subtracting the obtained capacitive current from the total measured current, the resistive current can be found.

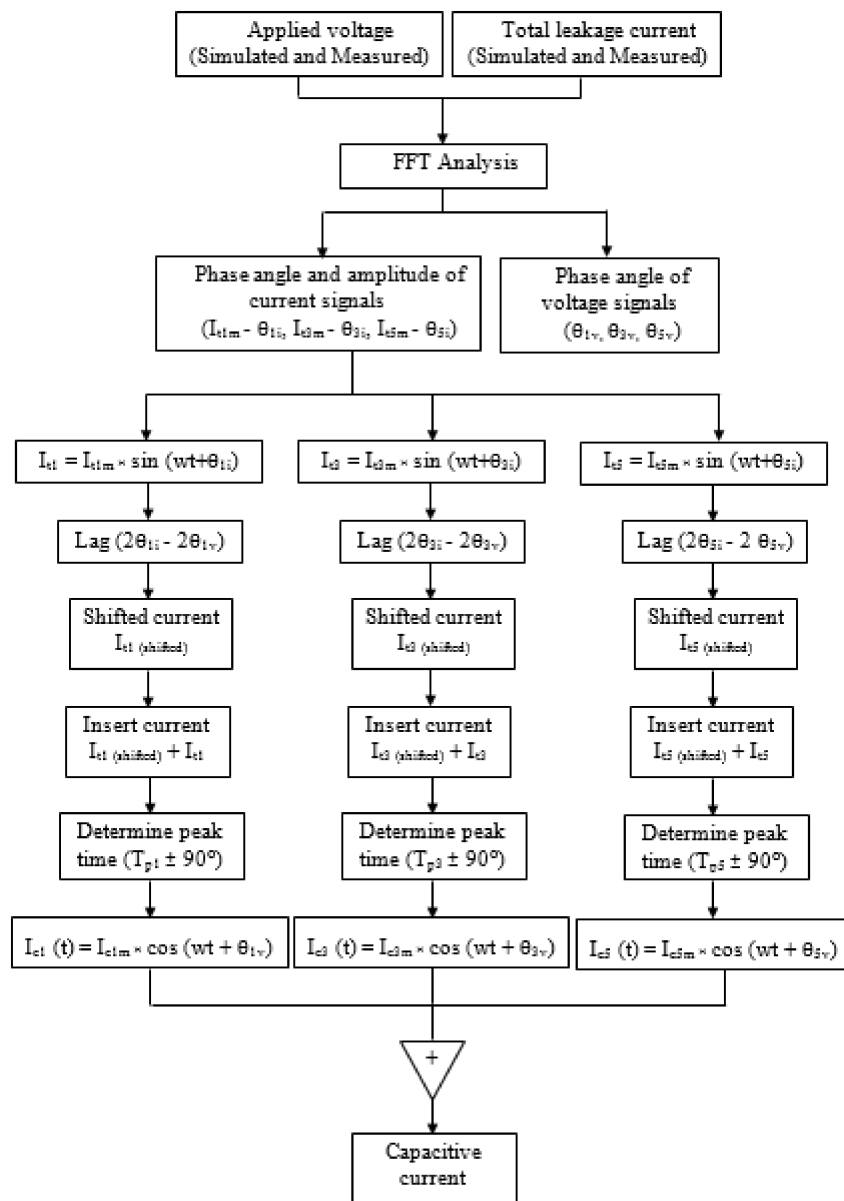


Figure 5. Block diagram of ITDAM steps.

3. Results and Discussion

This section presents the results that have been obtained from this work and the explanation of each result. These include the leakage current measurement results and comparison of leakage current amplitudes and signals between the measurement and simulation results.

3.1. Leakage Current under Different Applied Voltage Amplitude

The comparison between measurement and simulation results of the surge arrester total leakage current under different applied voltage amplitudes is shown in Figure 6, while the resistive and capacitive leakage currents are shown in Figure 7, respectively. Voltages from 6 kV to 10 kV were applied. It was found that the leakage current increases when the applied voltage is increased. This is fundamentally due to the direct proportionality between the voltage and current with an equivalent impedance, which is produced by the constant capacitive impedance, Z ($I = V/Z$). The percentage error between the measurement and modelling was calculated based on Equation (7) and is stated in Figures 6 and 7 above the bar. The percentage of error is calculated using the following expression:

$$\text{Percentage of error (\%)} = \left| \frac{I_{FEA} - I_m}{I_m} \right| \times 100 \tag{7}$$

where I_{FEA} is the simulated value of the surge arrester leakage current in μA and I_m is the measurement value of the surge arrester leakage current. According to the results, the average errors between the measurement and simulation for the total, resistive and capacitive leakage current are 1.60%, 4.05% and 1.38% respectively. This indicates that the measurement and simulation results are in good agreement with each other. Therefore, the proposed model of the surge arrester in this work under various applied voltage amplitudes can be considered reasonable.

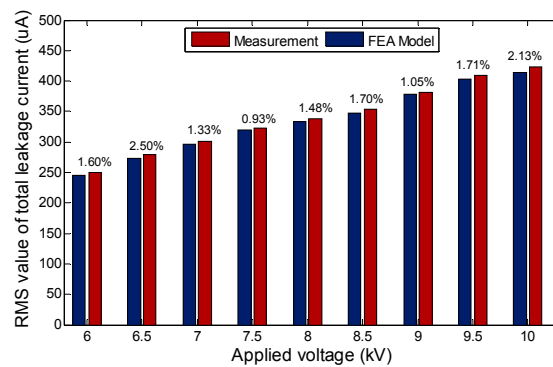


Figure 6. Comparison of RMS value of total leakage current between measurement and FEA model under different applied voltage amplitudes.

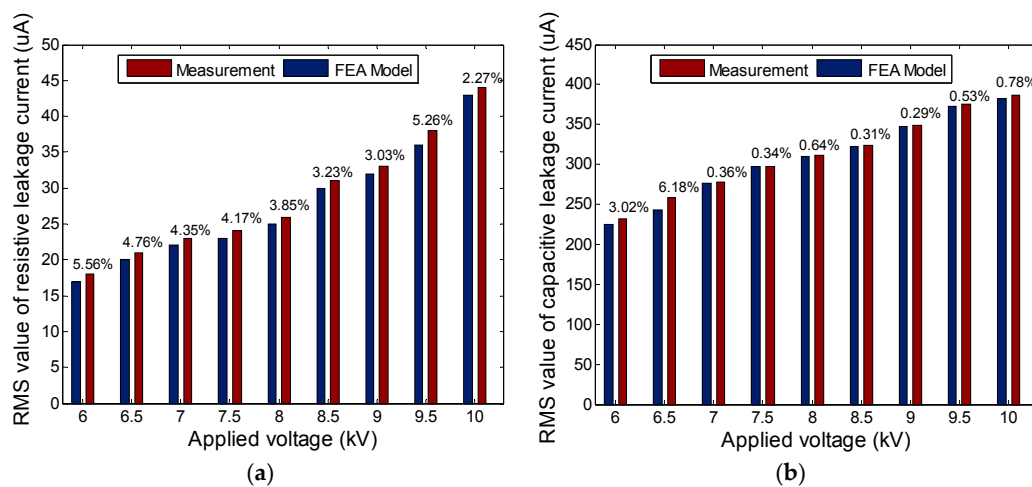


Figure 7. Comparison of RMS value of (a) resistive; (b) capacitive leakage current between measurement and FEA model under different applied voltage amplitudes.

In Figure 8, the waveforms of 10 kV_{rms} applied voltage, total leakage current, capacitive leakage current and resistive leakage current with harmonic components of total leakage current obtained using the ITDAM and FFT methods are shown. Figure 8a presents the results from the measurement while Figure 8b presents the FEA model results. According to the obtained measurement and simulation results, it can be seen that the developed FEA model is able to include harmonic components, producing reasonable results compared to the measurement results. The value of the resistive leakage current is 44 μ A from the measurement, which is around 7.7% of the total leakage current. The value of the resistive leakage current at 10 kV_{rms} from the FEA model is 43 μ A. This indicates that the difference between the measured and simulated resistive leakage current is only 3.8%.

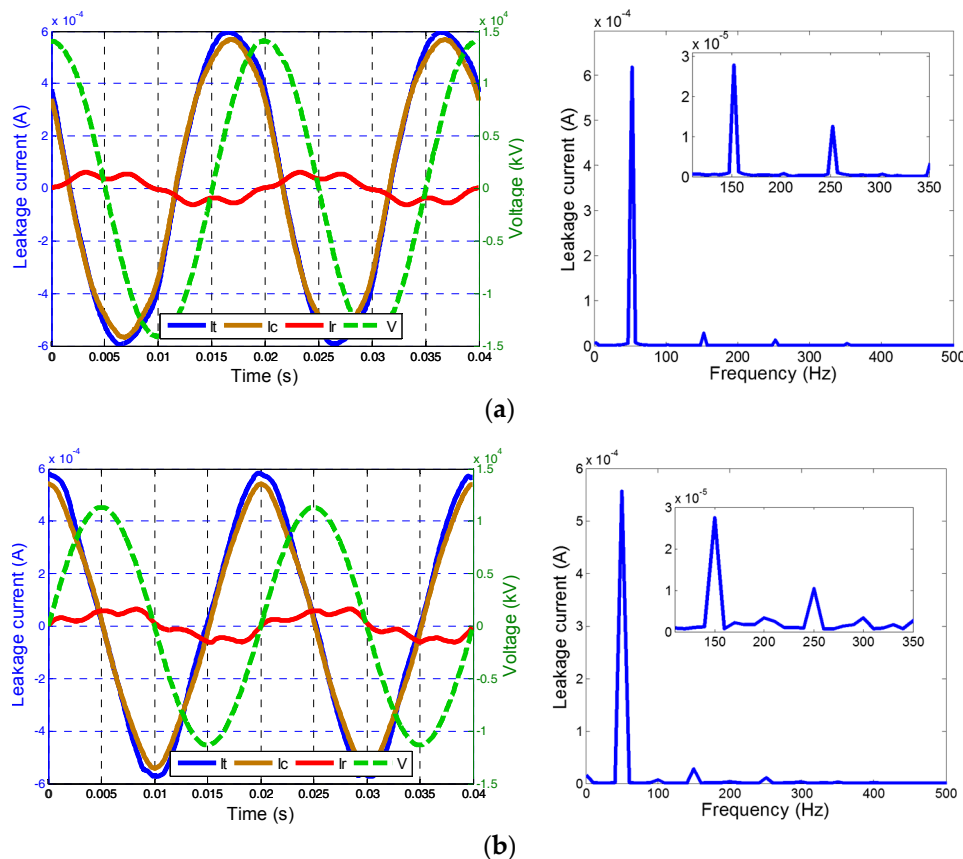


Figure 8. Leakage current waveforms and harmonic components at 10 kV_{rms} applied voltage from the (a) measurement; (b) FEA model.

3.2. Leakage Current under Different Wetness Conditions

The surge arrester was tested under different wetness conditions at 8 kV_{rms} and at 26 °C. Figure 9 shows the results of total leakage current value from measurement and simulation using the FEA model. From the results, it can be seen that the leakage current increases slightly when the arrester condition is wetter. This is due to the presence of more water droplets, which increase the conductivity along the surge arrester surface, providing an easier path for current to flow in the form of the negatively and positively charged ions that are moving from one electrode to the other electrode. Figure 10 shows the resistive and capacitive current components from the measured and simulated total leakage current. It can be seen that the resistive current component increases when there is more amount of water on the arrester surface. This humidification can also lead to moisture ingress into the surge arrester and degrade the lifetime of the surge arrester [30]. However, there is not much variation in the capacitive current components under different wetness conditions. The error between the measurement and simulation results using the FEA model is also shown in Figures 9 and 10. The average percentage

errors between the measurement and simulation results determined by Equation (7) are 1.03% for the total leakage current are 3.38% and 0.87% for resistive leakage current and capacitive leakage current, respectively.

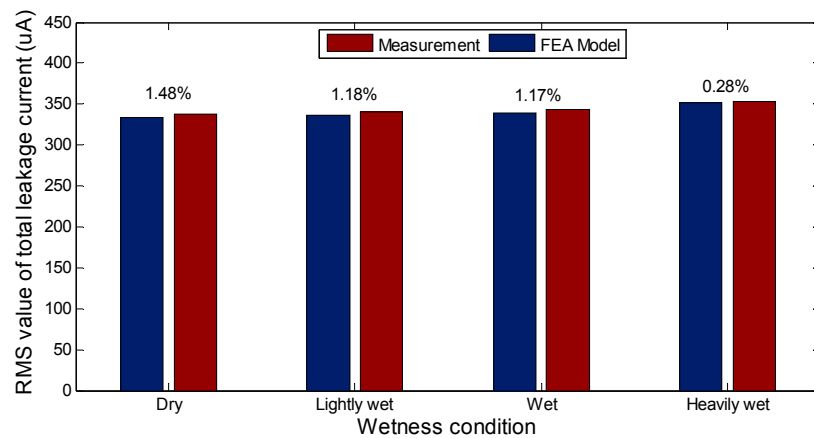


Figure 9. RMS value of the total leakage current between measurement and FEA model under different wetness conditions at 8 kV_{rms} .

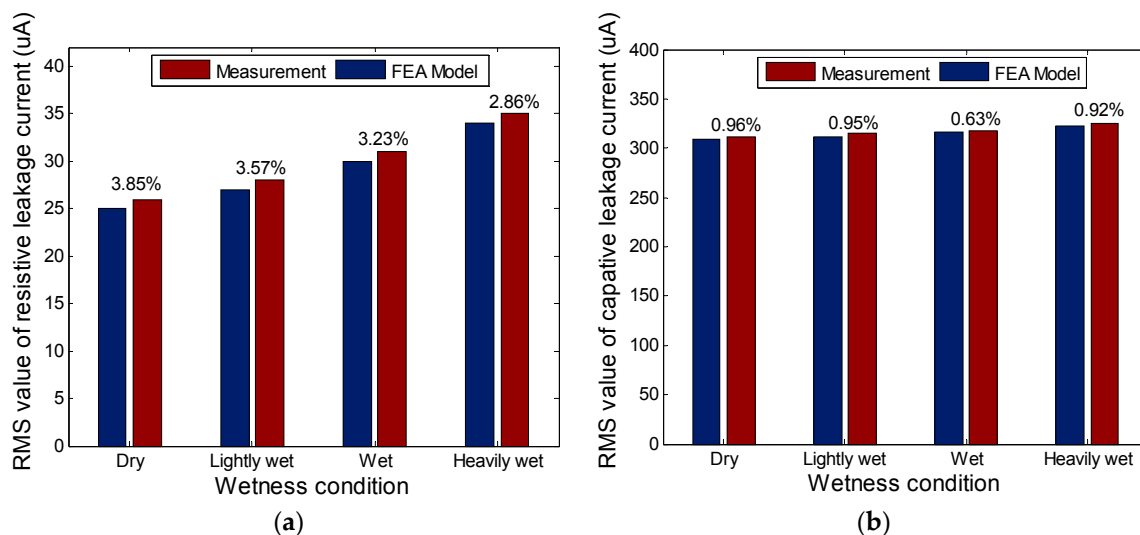


Figure 10. RMS value of the leakage current between measurement and FEA model under different wetness conditions at 8 kV_{rms} for (a) resistive; (b) capacitive leakage current.

In Figure 11a,b, the waveforms of 8 kV_{rms} applied voltage, total leakage current, capacitive leakage current and resistive leakage current with harmonic components of total leakage current for heavily wet surge arrester surface are presented. Figure 11 shows the results from the measurement while Figure 11b presents the FEA model results. The total leakage currents for the measurement and FEA model for heavily wet surge arrester are $352\text{ }\mu\text{A}$ and $351\text{ }\mu\text{A}$ while for the capacitive and resistive leakage currents are $322\text{ }\mu\text{A}$, $320\text{ }\mu\text{A}$, $34\text{ }\mu\text{A}$ and $33\text{ }\mu\text{A}$ accordingly. In general, the FEA model exhibits similar residual voltage patterns, which are in good agreement with the measurement. This indicates that the measurement and simulation results are in good agreement with each other. With a small relative error mostly caused by non-linear V-I characteristic settings, it can be assumed that the developed FEA model is sufficient in term of approximating the voltage distribution and current density of the surge arrester during normal operation conditions.

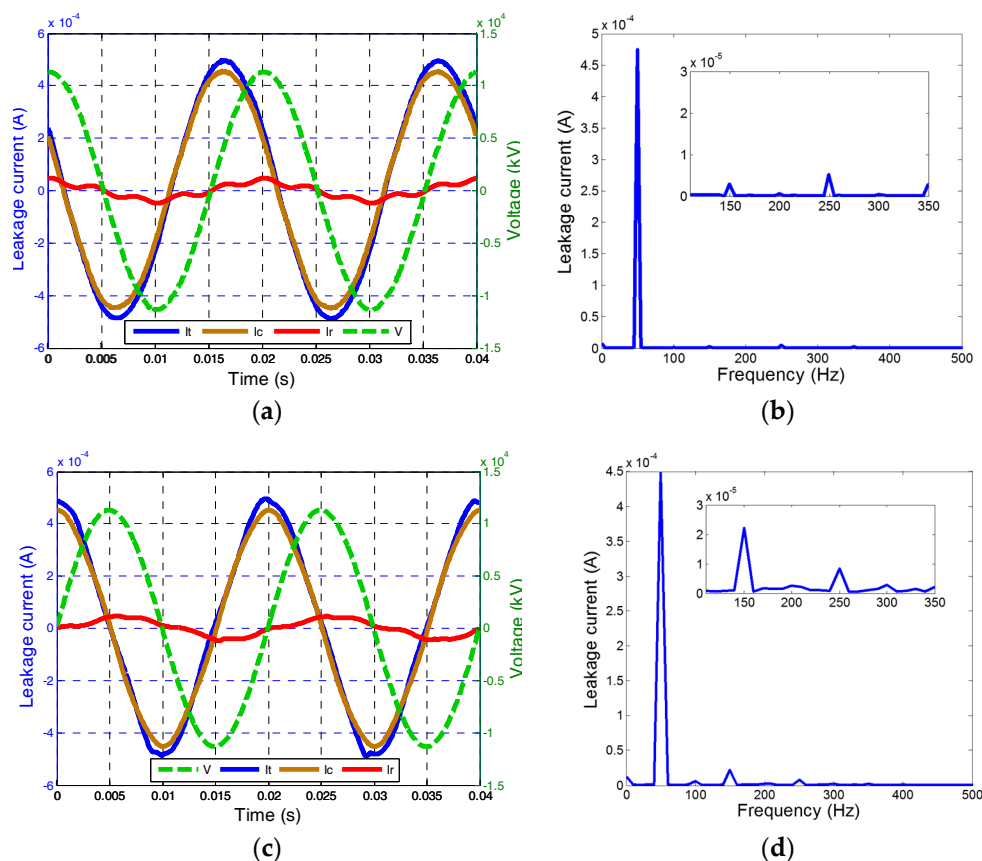


Figure 11. Leakage current waveforms and harmonic components at $8 \text{ kV}_{\text{rms}}$ applied voltage with heavily wet condition of surge arrester from the (a) measurement; (b) FEA model.

3.3. Leakage Current under Different Pollution Conditions

The leakage current behaviour of the surge arrester under different pollution conditions is shown in Figures 12 and 13. From the measurement, the surface of the surge arrester was contaminated with dry sand, wet sand, salt sand and salt water. The salt sand is a blend of normal sand and salt, NaCl, with ratio of 2:1 while the salt water is an emulsion of NaCl and water with ratio of 1:1 with NaCl solution conductivity of 88 mS/cm . From the results, the presence of salt sand, salt water and wet sand on the surge arrester surface increases the total leakage current along the arrester surface. This is due higher conductivity along the surge arrester surface provided by the salt and water, providing easier path for current to flow.

The resistive leakage current of salt water in Figure 13b shows the highest value, which suggests a high conductivity that can lead to arrester degradation. The free ions created when salts are dissolved in the water will freely dissociate into ions. The Na^+ and Cl^- ions are moving through the water containing charges and therefore they conduct the electricity. Dry sand does not cause the leakage current to increase significantly because it has low conductivity. It can be concluded that increasing of leakage current is correlated to the increment of surface conductivity in pollution conditions [23,31]. The error between the measurement and simulation results using the FEA model is also shown in Figures 12 and 13. The average percentage of error is 1.40% for the total leakage current, 3.71% for resistive leakage current and 0.79% for capacitive leakage current. This shows that the measurement and simulation results are in good agreement with each other.

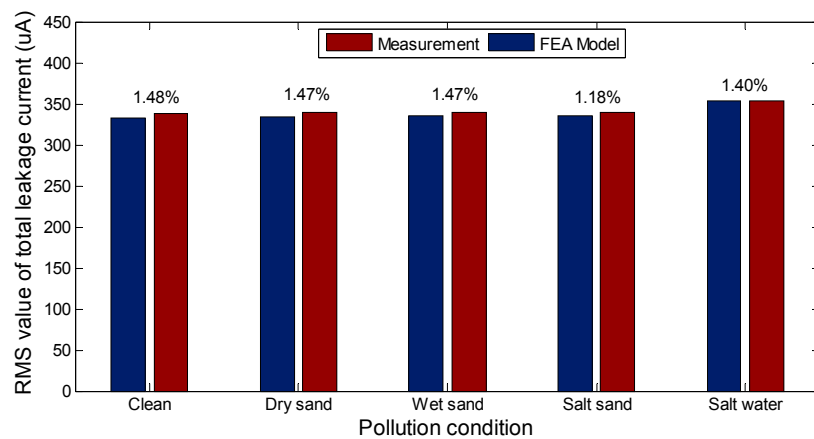


Figure 12. Comparison of RMS value of total leakage current between measurement and FEA model under different artificial pollution conditions.

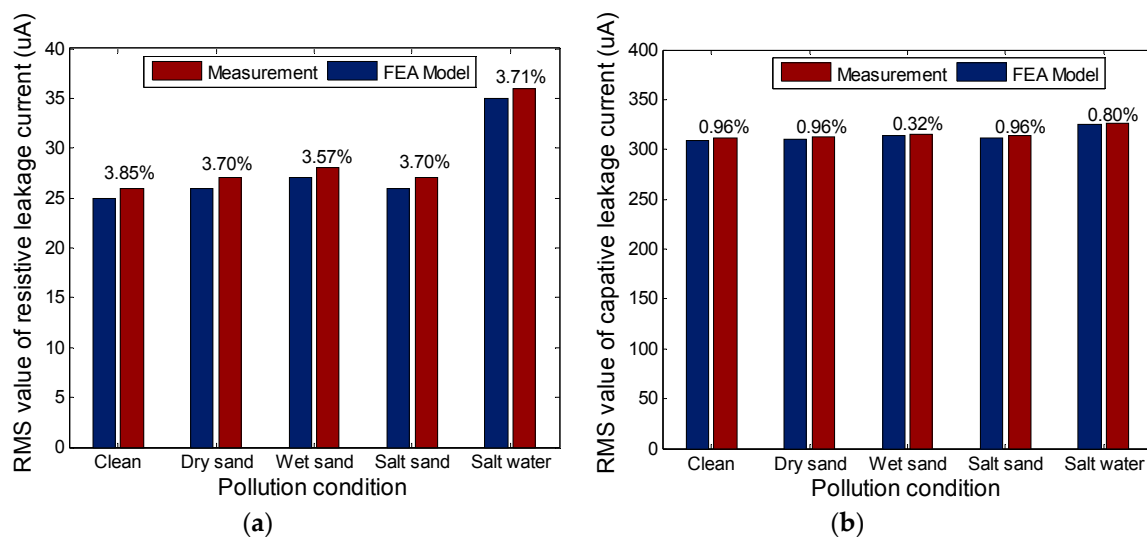


Figure 13. Comparison of RMS value of leakage current between measurement and FEA model under different artificial pollution conditions at 8 kV_{rms} (a) Resistive; (b) Capacitive.

The waveforms for the surge arrester polluted with salt water at 8 kV_{rms} applied voltage, total leakage current, resistive and capacitive leakage current are presented in Figure 14 with their harmonic components for measurement and FEA model. The total, capacitive and resistive leakage currents for measurement are 354, 326 and 36 μ A whereas they are 353, 325 and 35 μ A for the FEA model. The total, capacitive and resistive leakage currents increase around 16, 14 and 10 μ A accordingly from the clean surface surge arrester. From the obtained harmonic waveform as described in Figure 14, it can be realised that the fundamental, third and fifth harmonics influence the amplitude of the total leakage current under pollution with salt water. The increase of harmonic components and resistive current can lead to power loss, increase the temperature and therefore degrade the material that will possibly explode the surge arrester due to thermal avalanche.

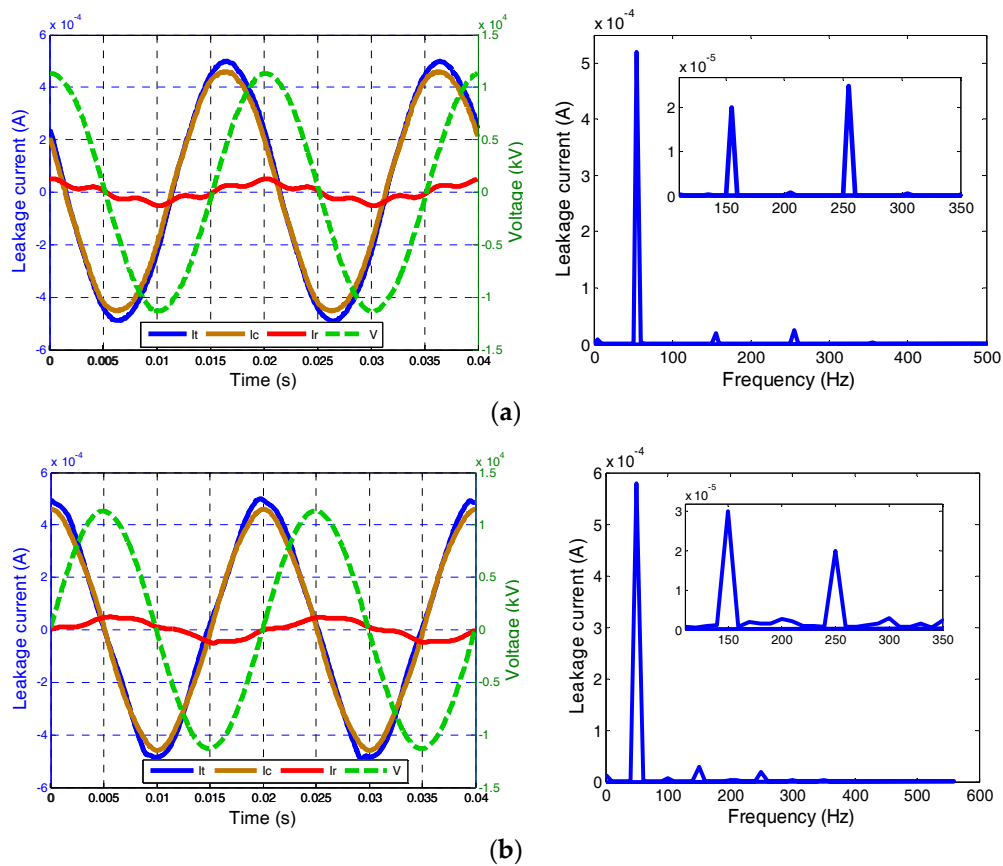


Figure 14. Leakage current waveforms and harmonic components at $8 \text{ kV}_{\text{rms}}$ applied voltage with salt water on the surge arrester from the (a) measurement; (b) FEA model.

4. Influence of Pollution on Leakage Current Harmonics

Since the polluted surface of the surge arrester influences the fundamental and third harmonic of the total leakage current [30,32], Fast Fourier transform (FFT) was used to obtain the harmonic components on the surge arrester under salt water pollution at $8 \text{ kV}_{\text{rms}}$. The results were compared with the clean surge arrester. Figure 15 presents the harmonic components of the total leakage current for the fundamental and third harmonic of the surge arrester with clean and polluted surge arrester surface with salt water for the surge arrester model.

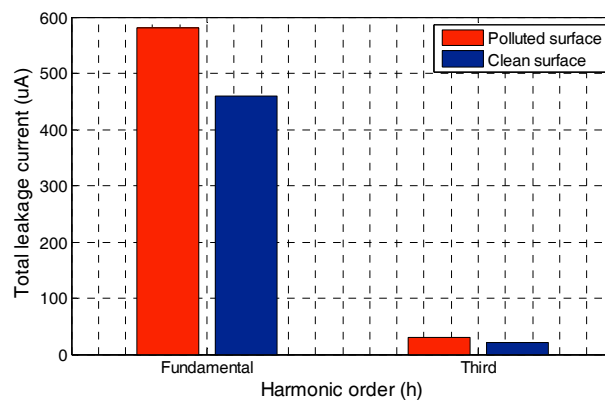


Figure 15. Harmonic components at $8 \text{ kV}_{\text{rms}}$ under clean and polluted surface.

From the obtained results, the magnitude of the fundamental and third harmonic for clean surge arrester is smaller than under the polluted condition. A rapid increase of leakage current on polluted surface of surge arrester is caused by the moist surface that leads to ionization of salts [33]. The percentage increases around 21.42% for the fundamental harmonic when the surge arrester was polluted with salt water. For the third harmonic under polluted surface conditions, the percentage increases to 26.67%. In general, it can be seen that the pollution influences the harmonics of leakage current, which can degrade the surge arrester performance.

5. Electric Field and Current Density Distributions in FEA Model

By using the FEA model, the distribution of electric potential, electric field and current density of the 11 kV surge arrester can be easily determined. Figure 16 presents the electric potential, current density and electric field distributions obtained from the FEA model at 9 kV_{rms} applied voltage amplitude and temperature of 26 °C. Referring to Figure 16a,b, the potential and current density distributions show that the highest potential is located at the top terminal of the arrester due to the applied high voltage, but decreases towards the bottom terminal, which is grounded. The same goes for Figure 16c where the electric field magnitude is the highest at the top terminal of the arrester due to the applied high voltage [26]. This is shown by the red colour scale for the electric potential and current density and more contour lines for the electric field. There is also relatively higher electric field magnitude on the top and bottom surfaces of each housing shed than in the surrounding housing. The electrical characteristics of the material and the geometry of the surge arrester also affect the distribution of the electric field [34].

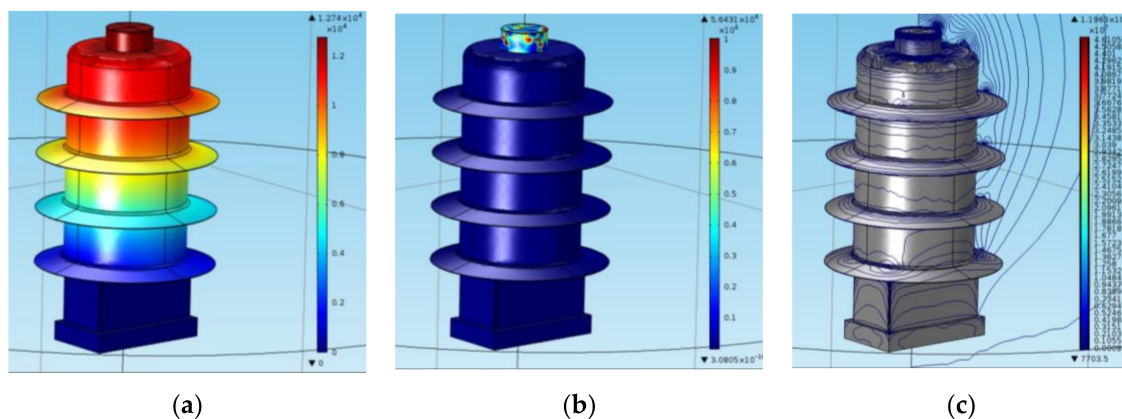


Figure 16. (a) Electric potential; (b) current density; (c) electric field distributions form the FEA model.

6. Conclusions

In this work, the effect of different applied voltage amplitudes, wetness conditions and pollution conditions on the surge arrester leakage current has been successfully evaluated using measurements and simulation models. It was found that the leakage current increases when the applied voltage amplitude is higher, wetness is higher and pollution conditions are worse.

A three-dimensional, 11 kV surge arrester model was successfully developed by finite element analysis (FEA) and was employed to obtain the total, resistive and capacitive leakage currents during normal operation under different conditions of applied voltage, wetness and pollution. The model was used to identify the surge arrester parameters which are influenced by these conditions. The leakage current amplitudes and signals obtained from the simulation of FEA model were also compared with the measurement results. It was found that the results obtained using the proposed FEA model are within reasonable agreement with the measurement results. Thus, the proposed FEA model for leakage current modelling in surge arrester in this work can be considered reasonable.

From the FEA model of the surge arrester that has been developed, it was found that the material conductivity affects the leakage current significantly under different applied voltage amplitude, wetness conditions and pollution conditions. Hence, physical parameters of the surge arrester that influence the leakage current under different conditions of the surge arrester have been identified from the FEA model. The proposed model can also help in improvement of surge arrester design through the assessment of leakage current.

Acknowledgments: The authors thank the University of Malaya, Malaysia and Malaysian Ministry of Higher Education (MOHE) for supporting this work through research grants of HIR (grant No.: H-16001-00-D000048) and PPP (grant No.: PPP 2016A-PG236).

Author Contributions: N.A.A.L., H.A.I. and A.H.A.B. conceived and designed the research methodologies; S.Z.A.D. and N.A.A.L. performed the experiments and analyzed the data; N.A.A.L. and H.A.I. wrote the paper.

Conflicts of Interest: The authors declare no conflict of interest.

References

1. Abu Bakar, A.; Zali, S.; Tan, C.K.; Ilias, H.; Mokhlis, H. A comparative study for current transformer dimensioning in overcurrent relay. *IEEJ Trans. Electr. Electron. Eng.* **2016**, *11*, S43–S48. [[CrossRef](#)]
2. Badran, O.; Mekhilef, S.; Mokhlis, H.; Dahalan, W. Optimal reconfiguration of distribution system connected with distributed generations: A review of different methodologies. *Renew. Sustain. Energy Rev.* **2017**, *73*, 854–867. [[CrossRef](#)]
3. Zaini, N.H.; Ab Kadir, M.Z.A.; Mohd Radzi, M.A.; Izadi, M.; Azis, N.; Ahmad, N.I.; Nasir, M.S.M. Lightning Surge Analysis on a Large Scale Grid-Connected Solar Photovoltaic System. *Energies* **2017**, *10*, 2149. [[CrossRef](#)]
4. Gatta, F.M.; Geri, A.; Lauria, S.; Maccioni, M. Monte Carlo evaluation of the impact of subsequent strokes on backflashover rate. *Energies* **2016**, *9*, 139. [[CrossRef](#)]
5. Shariatinasab, R.; Ajri, F.; Daman-Khorshid, H. Probabilistic evaluation of failure risk of transmission line surge arresters caused by lightning flash. *IET Gener. Transm. Distrib.* **2014**, *8*, 193–202. [[CrossRef](#)]
6. Shariatinasab, R.; Safar, J.G.; Falaghi, H. Optimisation of arrester location in risk assessment in distribution network. *IET Gener. Transm. Distrib.* **2014**, *8*, 151–159. [[CrossRef](#)]
7. Christodoulou, C.A.; Vita, V.; Perantzakis, G.; Ekonomou, L.; Milushev, G. Adjusting the Parameters of Metal Oxide Gapless Surge Arresters' Equivalent Circuits Using the Harmony Search Method. *Energies* **2017**, *10*, 2168. [[CrossRef](#)]
8. Ohki, Y. Advanced Directly Molded Type Polymer-Housed Surge Arresters. *IEEE Electr. Insul. Mag.* **2013**, *29*, 63–64. [[CrossRef](#)]
9. Vita, V.; Christodoulou, C.A. Comparison of ANN and finite element analysis simulation software for the calculation of the electric field around metal oxide surge arresters. *Electr. Power Syst. Res.* **2016**, *133*, 87–92. [[CrossRef](#)]
10. Woodworth, J. History of Arresters on Power Systems 1965—Present. 2011, pp. 1–8. Available online: http://www.arresterworks.com/history/pdf_files/History_of_Arresters_on_Power_Systems_1965-Present.pdf (accessed on 2 March 2018).
11. Sarajčev, P.; Goić, R. A review of current issues in state-of-art of wind farm overvoltage protection. *Energies* **2011**, *4*, 644–668. [[CrossRef](#)]
12. Vita, V.; Mitropoulou, A.; Ekonomou, L.; Panetsos, S.; Stathopoulos, I. Comparison of metal-oxide surge arresters circuit models and implementation on high-voltage transmission lines of the Hellenic network. *IET Gener. Transm. Distrib.* **2010**, *4*, 846–853. [[CrossRef](#)]
13. Lee, B.H.; Kang, S.M.; Eom, J.H.; Kawamura, T. A Monitoring Device of Leakage Currents Flowing through ZnO Surge Arresters. *Jpn. Soc. Appl. Phys.* **2003**, *42*, 1568. [[CrossRef](#)]
14. Lee, B.-H.; Kang, S.-M. A new on-line leakage current monitoring system of ZnO surge arresters. *Mater. Sci. Eng. B* **2005**, *119*, 13–18. [[CrossRef](#)]
15. Christodoulou, C.A.; Avgerinos, M.V.; Ekonomou, L.; Gonos, I.F.; Stathopoulos, I.A. Measurement of the resistive leakage current in surge arresters under artificial rain test and impulse voltage subjection. *IET Sci. Meas. Technol.* **2009**, *3*, 256–262. [[CrossRef](#)]

16. Xu, Z.N.; Zhao, L.J.; Ding, A.; Lu, F.C. A Current Orthogonality Method to Extract Resistive Leakage Current of MOSA. *IEEE Trans. Power Deliv.* **2013**, *28*, 93–101. [[CrossRef](#)]
17. Lundquist, J.; Stenstrom, L.; Schei, A.; Hansen, B. New method for measurement of the resistive leakage currents of metal-oxide surge arresters in service. *IEEE Trans. Power Deliv.* **1990**, *5*, 1811–1822. [[CrossRef](#)]
18. Luo, Y.F. Study on Metal-Oxide-Arrester on-Line Monitoring Distributed-Control-System. Master's Thesis, School Electrical Engineering, Xi'an Jiao Tong University, Xi'an, China, 2003.
19. Zhu, H.; Raghuvver, M.R. Influence of representation model and voltage harmonics on metal oxide surge arrester diagnostics. *IEEE Trans. Power Deliv.* **2001**, *16*, 599–603. [[CrossRef](#)]
20. Shirakawa, S.; Endo, F.; Kitajima, H.; Kobayashi, S.; Goto, K.; Sakai, M. Maintenance of surge arrester by a portable arrester leakage current detector. *IEEE Trans. Power Deliv.* **1988**, *3*, 998–1003. [[CrossRef](#)]
21. Heinrich, C.; Hinrichsen, V. Diagnostics and monitoring of metal-oxide surge arresters in high-voltage networks-comparison of existing and newly developed procedures. *IEEE Trans. Power Deliv.* **2001**, *16*, 138–143. [[CrossRef](#)]
22. Khodsuz, M.; Mirzaie, M. An improved time-delay addition method for MOSA resistive leakage current extraction under applied harmonic voltage. *Measurement* **2016**, *77*, 327–334. [[CrossRef](#)]
23. Khodsuz, M.; Mirzaie, M. Evaluation of ultraviolet ageing, pollution and varistor degradation effects on harmonic contents of surge arrester leakage current. *IET Sci. Meas. Technol.* **2015**, *9*, 979–986. [[CrossRef](#)]
24. Khodsuz, M.; Mirzaie, M. Harmonics ratios of resistive leakage current as metal oxide surge arresters diagnostic tools. *Measurement* **2015**, *70*, 148–155. [[CrossRef](#)]
25. Seyyedbarzegar, S.M.; Mirzaie, M. Thermal balance diagram modelling of surge arrester for thermal stability analysis considering ZnO varistor degradation effect. *IET Gener. Transm. Distrib.* **2016**, *10*, 1570–1581. [[CrossRef](#)]
26. Illias, A.Z.; Halim, S.A.; Bakar, A.H.A.; Mokhlis, H. Determination of surge arrester discharge energy using finite element analysis method. *IET Sci. Meas. Technol.* **2014**, *9*, 693–701. [[CrossRef](#)]
27. Bakar, A.; Halim, A.; Zainal Abidin, A.; Illias, H.A.; Mokhlis, H.; Abd Halim, S.; Nor Hassan, N.H.; Tan, C.K. Determination of the striking distance of a lightning rod using finite element analysis. *Turk. J. Electr. Eng. Comput. Sci.* **2016**, *24*, 4083–4097. [[CrossRef](#)]
28. Illias, H.; Chen, G.; Lewin, P.L. Comparison between three-capacitance, analytical-based and finite element analysis partial discharge models in condition monitoring. *IEEE Trans. Dielectr. Electr. Insul.* **2017**, *24*, 99–109. [[CrossRef](#)]
29. Illias, H.A.; Chen, G.; Lewin, P.L. The influence of spherical cavity surface charge distribution on the sequence of partial discharge events. *J. Phys. D Appl. Phys.* **2011**, *44*, 245202. [[CrossRef](#)]
30. Metwally, I.A.; Eladawy, M.; Feilat, E.A. Online Condition Monitoring of Surge Arresters Based on Third-Harmonic Analysis of Leakage Current. *IEEE Trans. Dielectr. Electr. Insul.* **2017**, *24*, 2274–2281. [[CrossRef](#)]
31. Faria, I.P.D.; Martinez, M.L.B.; Queiroz, A.A.A.D. Electrical performance evaluation of plasticized polyolefin formulation developed for manufacturing surge arresters housings. *IEEE Trans. Dielectr. Electr. Insul.* **2015**, *22*, 3429–3441. [[CrossRef](#)]
32. Khodsuz, M.; Mirzaie, M. Monitoring and identification of metal-oxide surge arrester conditions using multi-layer support vector machine. *IET Gener. Trans. Distrib.* **2015**, *9*, 2501–2508. [[CrossRef](#)]
33. Chen, W.; Wang, W.; Xia, Q.; Luo, B.; Li, L. Insulator contamination forecasting based on fractal analysis of leakage current. *Energies* **2012**, *5*, 2594–2607. [[CrossRef](#)]
34. Abdul Latiff, N.A.; Illias, H.; Abu Bakar, A.H.; Abd Halim, S.; Dabbak, S.Z. Design technique for leakage current reduction in surge arrester using gravitational search algorithm and imperialist competitive algorithm. *Int. J. Comput. Math. Electr. Electron. Eng.* **2018**, *37*, 357–374. [[CrossRef](#)]

